Symmetric and antisymmetric nonlinear modes supported by dual local gain in lossy lattices

K. W. Chow,[1] Edwin Ding,[2] Boris A. Malomed,[3] and A. Y. S. Tang[1]
[1] *Department of Mechanical Engineering, University of Hong Kong, Pokfulam Road, Hong Kong*
[2] *Department of Mathematics and Physics, Azusa Pacific University, Box 7000, Azusa, CA 91702-7000, USA*
[3] *Department of Physical Electronics, School of Electrical Engineering, Faculty of Engineering, Tel Aviv University, Tel Aviv 69978, Israel*

We introduce a discrete lossy system, into which a double "hot spot" (HS) is inserted, i.e., two mutually symmetric sites carrying linear gain and cubic nonlinearity. The system can be implemented as an array of optical or plasmonic waveguides, with a pair of amplified nonlinear cores embedded into it. We focus on the case of the self-defocusing nonlinearity and cubic losses acting at the HSs. Symmetric localized modes pinned to the double HS are constructed in an implicit analytical form, which is done separately for the cases of odd and even numbers of intermediate sites between the HSs. In the former case, some stationary solutions feature a w-like shape, with a low peak at the central site, added to tall peaks at the positions of the embedded HSs. The special case of two adjacent HSs is considered too. Stability of the solution families against small perturbations is investigated in a numerical form, which reveals stable and unstable subfamilies. The instability generated by an isolated positive eigenvalue leads to a spontaneous transformation into a co-existing stable mode, while a pair of complex-conjugate eigenvalues gives rise to persistent breathers.

I. INTRODUCTION

Dissipative solitons, which originate, in the spatial domain, from the simultaneous balance between diffraction and self-focusing, and between gain and loss, are the subject of fundamental importance in optics [1] and plasmonics [2, 3]. An obvious condition necessary for the stability of dissipative bright solitons is the stability of the zero solution, i.e., background around the soliton. This condition may be satisfied by linearly coupled complex Ginzburg-Landau (CGL) equations [4], which describe dual-core waveguides, with the linear gain applied to an active core, while the parallel-coupled passive one is lossy [3, 5–7]. The stability of dissipative solitons can be also provided by the single CGL equation including the linear loss, cubic gain and quintic loss [8, 9].

Recently, considerable attention was drawn to another method of the creation of stable localized dissipative modes, using linear gain localized at a "hot spot" (HS) [10–13]. Configurations with multiple HSs [14–16], as well as with extended amplifying structures [17], have been introduced too. Such settings can be created by implanting gain-producing dopants into a narrow segment of the waveguide [18], or by focusing an external pumping beam at the target spot(s) in a uniformly-doped waveguide.

Solutions for dissipative solitons pinned to narrow HSs approximated by delta-functions have been found in an analytical form [11, 14, 16]. More sophisticated one- and two-dimensional localized modes, such as vortices supported by the gain acting in a ring-shaped area [19], have been found in the numerical form [12, 13, 15].

A natural setting for the implementation of the HS is provided by discrete systems, i.e., lossy multi-core waveguiding arrays, where the gain is applied to a single selected core. Assuming that the nonlinearity is also concentrated at the pumped core, while the bulk of the array is linear, exact solutions for modes pinned to the HS in such a system were recently found in an implicit analytical form in Ref. [20], and stability boundaries for the solutions were identified in a numerical form, in the parameter plane of the linear gain and cubic loss (or gain) acting at the HS. In particular, it was demonstrated that the pinned modes may be *stable*, under the combined action of the *unsaturated* cubic gain (in the absence of quintic losses) and cubic self-defocusing nonlinearity, which is impossible in uniform dissipative media (but possible in the case of the localized unsaturated cubic gain acing in a continuous medium [13]). On the other hand, it was demonstrated that the interplay of the linear gain, cubic loss, and cubic self-defocusing nonlinearity in the same system gives rise to a bistability, which is a noteworthy effect too.

The next natural step in the analysis of the discrete system is to investigate the one with two mutually symmetric HSs embedded into it, which is the subject of the present work. Previously, symmetric modes pinned to a pair of symmetric nonlinear sites implanted into a linear lattice were studied in Ref. [21], and exact solutions for stable asymmetric modes in the same system, generated by the respective symmetry-breaking bifurcation, were recently reported in Ref. [22].

The paper is organized as follows. The discrete CGL equation with the embedded double HSs, and its implicit analytical solutions for pinned modes are introduced in Sec. II. Numerical results, which include the linear-stability analysis of the analytically found stationary solutions and direct simulations of the underlying discrete CGL equation, are reported in Sec. III. Because the system features competition between the gain and loss, direct simulations converge

to attractors. In particular, the simulations allow us to identify stable modes into which unstable analytically found ones spontaneously transform. The paper is concluded by Sec. IV.

II. THE MODEL AND ANALYTICAL RESULTS

A. Formulation of the model

We consider the transmission of optical or plasmonic waves in a discrete array of linear lossy waveguides, with two identical embedded nonlinear pumped cores (alias HSs) embedded into it:

$$\frac{\mathrm{d}u_m}{\mathrm{d}z} = \frac{i}{2}\left(u_{m-1} - 2u_m + u_{m+1}\right) - \gamma u_m + \left[(\Gamma_1 + i\Gamma_2) + (iB - E)\left|u_m\right|^2\right]\left(\delta_{m,a} + \delta_{m,b}\right)u_m \ , \tag{1}$$

where z is the propagation distance, m the number of the waveguiding core, $u_m(z)$ the complex amplitude of the electromagnetic field in it, $\gamma \geq 0$ the linear-loss parameter, and the coefficient of the linear coupling between adjacent cores is scaled to be 1. Further, $\Gamma_1 > 0$ is the linear gain applied at the two HSs, which are represented by cores with numbers a and b (both numbers are integer), $\Gamma_2 \geq 0$ is the attractive potential which may be a part of the HS, $B > 0$ or $B < 0$ characterize the self-focusing or defocusing Kerr nonlinearity acting in the active cores, and $E > 0$ is the coefficient of the cubic loss. In light of the analysis performed in Ref. [20] for the discrete array with the single embedded HS, we focus below on the self-defocusing nonlinearity, fixing $B = -1$, as otherwise the pinned modes are prone to be unstable. However, it is necessary to present the analysis separately for the cases of odd and even numbers of sites separating the two HSs. It is expected that the two cases become similar for a sufficiently large separation.

B. An odd number of intermediate sites between the hot spots

To model the scenario with an odd number of sites between the two HSs, we set in Eq. (1) $a = N_0$ and $b = -N_0$, where $N_0 = 1, 2, 3, ...$ is a positive integer, and the number of the intermediate sites is $2N_0 - 1$. In this case, we look for a stationary solution to Eq. (1) in the form of

$$u_m = U_m e^{ikz}, \tag{2}$$

where a piecewise ansatz for the symmetric double-peak mode is

$$U_m = \begin{cases} Ae^{-\lambda|m|}, \text{ if } |m| \geq N_0 \ , \\ C\cosh(\lambda m), \text{ if } |m| < N_0 \ . \end{cases} \tag{3}$$

Here $\lambda \equiv \lambda_r + i\lambda_i$ is a complex eigenvalue, with $\lambda_r > 0$, and amplitude A may be defined to be real. Substituting this ansatz into Eq .(1) gives the following system of algebraic equations:

$$\begin{aligned} \cosh\lambda_r \cos\lambda_i - 1 &= k \ , \\ \sinh\lambda_r \sin\lambda_i &= -\gamma \ , \\ Ae^{-\lambda N_0} &= C\cosh(\lambda N_0) \ , \\ \Gamma_1 + i\Gamma_2 + (iB - E)|A|^2 e^{-2\lambda_r N_0} &= \frac{i}{2}\left(\frac{e^{\lambda} - e^{-\lambda}}{1 + e^{-2\lambda N_0}}\right) \ . \end{aligned} \tag{4}$$

This system, and its counterpart (8), derived below for the case of an even distance between the HSs, are referred to as *reduced models* in the rest of the paper. Equations (4) and (8) were solved numerically by means of the Newton's method.

Note that, in addition to the symmetric modes represented by ansatz (3), it is also possible to look for antisymmetric solutions, in the form of

$$U_m = \begin{cases} A\ \mathrm{sgn}(m)\ e^{-\lambda|m|}, \text{ if } |m| \geq N_0 \ , \\ C\sinh(\lambda m), \text{ if } |m| < N_0 \ . \end{cases} \tag{5}$$

An obvious difference between *ansätze* (3) and (5) is that the former one always has a nonzero amplitude at the center, $U_0 \equiv C \neq 0$, while the antisymmetric solution automatically vanishes at the central site ($U_0 = 0$). Antisymmetric modes will be considered in detail elsewhere, although numerically found examples are mentioned below, see the profiles depicted by the blue continuous line in the top left top panel of Fig. 4, and middle left panel of Fig. 8.

C. An even number of intermediate sites between the hot spots

In the case of an even number of sites between the HSs, we set in Eq. (1)

$$a = N_0,\ b = -N_0 + 1, \tag{6}$$

where $N_0 = 1, 2, 3, ...$ is again a positive integer, the corresponding number of intermediate sites between the HSs being $2\,(N_0 - 1)$. In this case we look for stationary solution (2) by means of the following piecewise ansatz, which symmetric about the off-site central point, $m = 1/2$:

$$U_m = \begin{cases} A\ e^{-\lambda(m-1/2)},\ \text{if}\ m \geq N_0, \\ A\ e^{\lambda(m-1/2)},\ \text{if}\ \ m \leq -N_0 + 1\ , \\ C\cosh\left(\lambda\left(m - 1/2\right)\right),\ \text{if}\ \ -N_0 + 1 < m < N_0\ . \end{cases} \tag{7}$$

With regard to this condition, substituting ansatz (7) into Eq. (1) leads to the following reduced system of equations:

$$\begin{gathered} \cosh\lambda_r \cos\lambda_i - 1 = k\ , \\ \sinh\lambda_r \sin\lambda_i = -\gamma\ , \\ A\ e^{-\lambda(N_0-1/2)} = C\cosh\left(\lambda\left(N_0 - \frac{1}{2}\right)\right)\ , \\ \Gamma_1 + i\Gamma_2 + (iB - E)|A|^2 e^{-2\lambda_r(N_0-1/2)} = \frac{i}{2}\left(\frac{e^{\lambda} - e^{-\lambda}}{1 + e^{-2\lambda(N_0-1/2)}}\right)\ . \end{gathered} \tag{8}$$

The first two equations in Eqs. (4) are identical to those in Eqs. (8), as they are derived in the bulk lattice, off the HS sites.

III. THE LINEAR-STABILITY ANALYSIS

The stability of the pinned modes was studied by means of the standard linearization procedure. To this end, perturbed solutions were taken as

$$u_m = \left[U_m + \epsilon V_m(z)\right] e^{ikz}, \tag{9}$$

where $V_m(z) \equiv X_m(z) + iY_m(z)$ is a complex perturbation with an infinitesimal amplitude $\epsilon \ll 1$. Substituting this into Eq. (1), we derive the following linearized equations:

$$\begin{gathered} \frac{\mathrm{d}X_m}{\mathrm{d}z} = -\frac{1}{2}Y_{m-1} + (k+1)Y_m - \frac{1}{2}Y_{m+1} - \gamma X_m \\ +(\delta_{m,a} + \delta_{m,b})\left\{(\Gamma_1 X_m - \Gamma_2 Y_m)\right. \\ -B\left[2P_m Q_m X_m + \left(P_m^2 + 3Q_m^2\right)Y_m\right] \\ \left.-E\left[\left(3P_m^2 + Q_m^2\right)X_m + 2P_m Q_m Y_m\right]\right\}\ , \\ \frac{\mathrm{d}Y_m}{\mathrm{d}z} = \frac{1}{2}X_{m-1} - (k+1)X_m + \frac{1}{2}X_{m+1} - \gamma Y_m \\ +(\delta_{m,a} + \delta_{m,b})\left\{(\Gamma_2 X_m + \Gamma_1 Y_m)\right. \\ +B\left[\left(3P_m^2 + Q_m^2\right)X_m + 2P_m Q_m Y_m\right] \\ \left.-E\left[2P_m Q_m X_m + \left(P_m^2 + 3Q_m^2\right)Y_m\right]\right\}\ , \end{gathered} \tag{10}$$

where $P_m \equiv \mathrm{Re}(U_m)$ and $Q_m \equiv \mathrm{Im}(U_m)$. An eigenvalue problem is obtained from here by substituting $X_m = \phi_m \exp(\rho z)$ and $Y_m = \psi_m \exp(\rho z)$ into Eqs. (10), where ρ is the instability growth rate. The pinned mode is linearly stable provided that all the eigenvalues have $\mathrm{Re}\,(\rho) \leq 0$.

IV. NUMERICAL RESULTS

A. An odd number of intermediate sites between the hot spots

The top panel of Fig. 1 shows a typical evolution of a discrete pulse in the self-defocusing case, $B = -1$, with the cubic loss, $E > 0$. When linear gain Γ_1 exceeds a certain threshold value, a randomly built initial profile evolves into

a stable two-peak solution, with peaks located at the HSs. The bottom panel of Fig. 1 shows agreement between the solutions produced by the direct simulations (the blue solid line) and the results obtained from the reduced system (4) (a chain of red crosses).

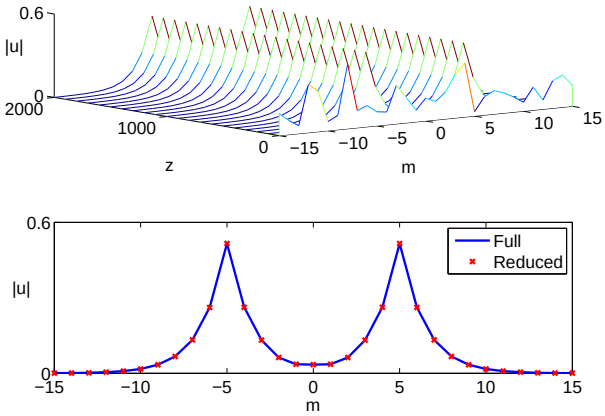

FIG. 1: (Color online) Top: Stable evolution of a random initial configuration into a stable two-peak mode (*attractor*) in the system with an odd number of intermediate sites between the hot spots. The two hot spots are located at $m = \pm 5$, with parameters $B = -1$, $E = 0.16$, $\Gamma_1 = 0.889$, $\Gamma_2 = 0.8$, and $\gamma = 0.5$. The computational domain used here is $-30 \leq m \leq 30$. Bottom: Solutions produced, as *attractors*, by direct simulations of Eq. (1) (the blue solid line), and those obtained from the reduced model (4) (red crosses). The blue curves and chains of red crosses have the same meaning in similar figures displayed below.

Next, we study the linear stability of the families of stationary pinned modes. First, we build a branch of the symmetric double-peak solutions in the form of ansatz (3) by means of a continuation algorithm applied to the reduced system (4). Figure 2 shows two main characteristics of the solution family, namely the peak amplitude, $A \exp(-\lambda_r N_0)$ (see Eqs. (3)), and the inverse width, λ_r, as functions of the linear gain, Γ_1. At $\Gamma_1 \leq 0.7284$, which is the above-mentioned threshold value, only the zero solution, with $A = C = 0$, is possible, as the system does not have enough gain to compensate the background loss and sustain any nontrivial solution. Double-peak modes exist at $\Gamma_1 > 0.7284$. We then computed the linear stability spectrum for each solution belonging to the branch, which allows one to identify stable (blue) and unstable (red) segments in Fig. 2. For the present set of the parameters, stable solutions were found in the regions of $0.7284 < \Gamma_1 \leq 0.9863$ (region I), $1.157 \leq \Gamma_1 \leq 1.254$ (region II), and $\Gamma_1 \geq 0.9508$ (region III). Unstable branches were found in the complementary segments, namely, $0.9863 < \Gamma_1 < 1.157$ (region IV) and $0.9508 < \Gamma_1 < 1.254$ (region V).

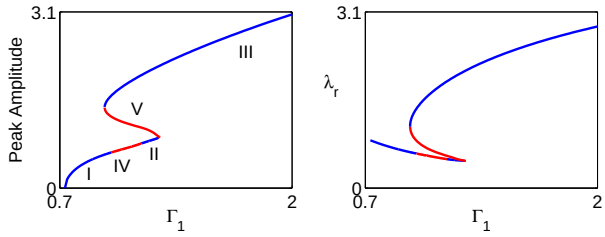

FIG. 2: (Color online) Characteristics of the family of symmetric double-peak stationary solutions, obtained from the reduced system (4) in the model with the odd number of intermediate sites between the hot spots, versus the linear gain, Γ_1. The parameters are $B = -1$, $E = 0.16$, $\Gamma_2 = 0.8$, $\gamma = 0.5$, and $N_0 = 5$. Here and in similar figures displayed below, blue and red segments designate linearly stable and unstable solutions, respectively, as identified from a numerical solution of the eigenvalue problem defined by Eqs. (10).

Further, left plots in Fig. 3 display examples of solutions obtained from direct simulations of Eq. (1) (blue solid curves), and their counterparts generated by reduced system (4) (red crosses), in stable regions I, II, and III, while right plots display the corresponding linear spectra. In stable region I (the top panel), the mode features the simple profile, with the peaks existing solely at the HS positions, $m = \pm 5$, and a minimum at the center ($m = 0$). In contrast

to that, in stable region II (the middle panel), the steady-state solution features a w-shaped profile, with an additional local peak appearing at $m = 0$. Note that reduced system (4) correctly predicts this more sophisticated profile. In stable region III (the bottom panel), two tall narrow peaks are, as a matter of fact, the same isolated solutions as those recently found in the single-HS model [20], with negligible interaction between them.

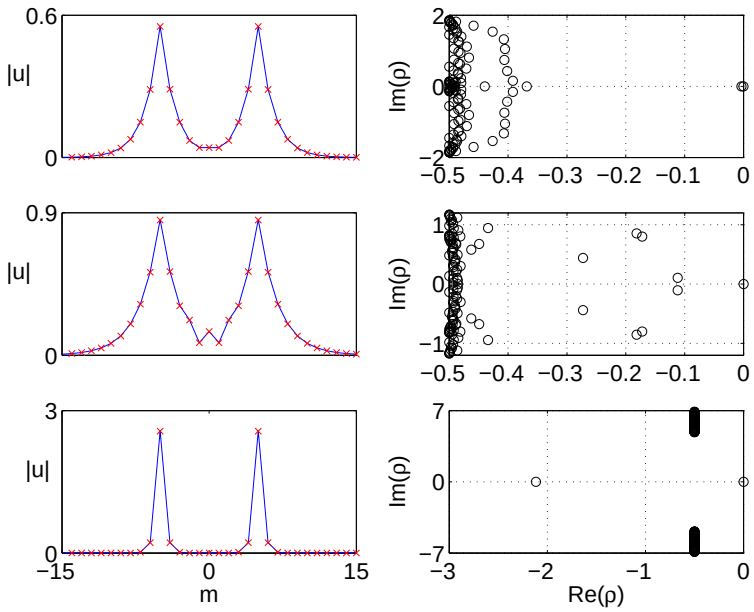

FIG. 3: (Color online) Left: Stable solutions produced by direct simulations of Eq. (1), and by the reduced model (4), at $\Gamma_1 = 0.9179$ (top), $\Gamma_1 = 1.2246$ (middle), and $\Gamma_1 = 1.5627$ (bottom), in the model with an odd number of intermediate sites. Other parameters are as in Fig. 2. Right: The corresponding linear-stability spectra.

Figure 4 shows solutions of the reduced model (red crosses) which turn out to be unstable, in segments IV and V of the solution branch (see Fig. 2). In the unstable region IV (the top row in the figure), the solutions of the reduced system (red crosses) feature a w-shaped profile, resembling the above-mentioned stable solution found in region II. However, as these solutions are unstable, they cannot be obtained by direct simulations of Eq. (1). In fact, at the same parameters, the full system evolves into a stable profile for which the amplitude at the central site, $m = 0$, is zero. This type of the solution cannot be described by ansatz (3), and it is plausible that it corresponds to the antisymmetric ansatz (5), which will be considered in detail elsewhere. In unstable region V (the bottom panels in Fig. 4), the two peaks in the unstable solution predicted by the reduced system interact with each other, featuring conspicuous overlap, whereas in the stable solution generated by the direct simulations for the same parameter set, the peaks are completely separated. In fact, in this case the stable solutions generated by the direct simulations evolve into the modes which exist, at the same parameters, in segment III on the stable branch (see Fig. 2).

We also studied the linear stability for different values of the linear background loss coefficient, γ. Figure 5 shows a set of solution branches for γ varying from 0.45 to 1.25. At lower values of the background loss (e.g., $0.4 \leq \gamma \leq 0.7$) the branches resemble the one shown above in Fig. 2, i.e., they consist of three stable and two unstable segments. When γ increases, the unstable segments shrink and eventually disappear. When this happens, the solutions become stable for all values of Γ_1. Note that the fully stable branches are single-valued, in contrast to multi-valued ones which include unstable segments.

Figure 6 shows typical solution branches obtained for still smaller levels of the background loss, $\gamma = 0.3$ and $\gamma = 0.2$ in the left and right panels, respectively. For the present values of the parameters, we have found two stable segments on the branches, with smaller and larger amplitudes, severally. Two typical solution profiles and their linear-stability spectra are shown in Fig. 7, while Fig. 8 shows unstable solutions belonging to the low-amplitude branch at $\gamma = 0.3$. The type of the instability revealed by the top and middle panels (represented by an isolated purely real positive eigenvalue) has already been seen in Fig. 4. However, a Hopf bifurcation, accounted for by pairs of complex eigenvalues, is observed at larger Γ_1 on the low-amplitude branch. Specifically, a pair of complex-conjugate eigenvalues crosses the imaginary axis into the right (unstable) half-plane. The Hopf bifurcation naturally leads to periodic oscillations, i.e., transformation of the unstable stationary mode into a persistent breather, which keeps the overall double-peak structure, see an example in the bottom row of Fig. 8.

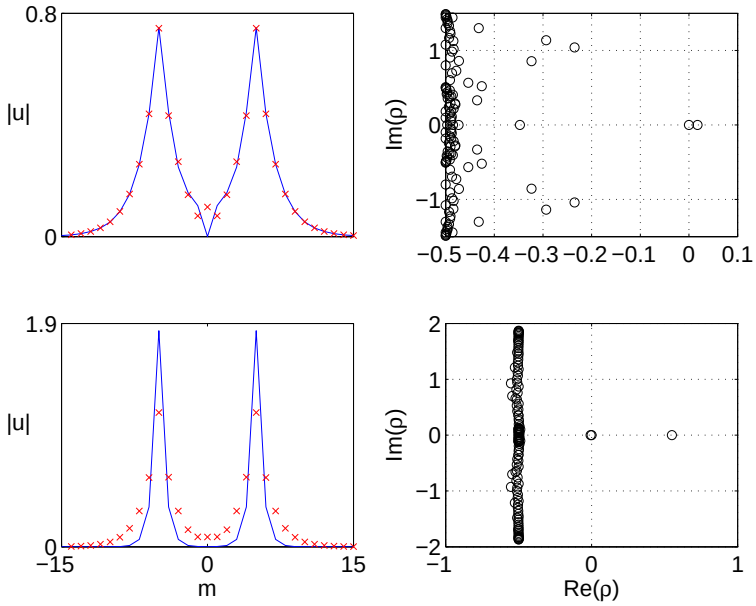

FIG. 4: (Color online) Left: Unstable solutions predicted by the reduced model with an odd number of intermediate sites (chains of red crosses), and actual stable solutions produced by direct simulations of Eq. (1) (blue solid curves) at $\Gamma_1 = 1.1186$ (top), and $\Gamma_1 = 1.0724$ (bottom). Right: The corresponding linear-instability spectra of the solutions obtained from the reduced system. Isolated eigenvalues with $\lambda_i = 0$ and $\lambda_r > 0$ indicate instabilities.

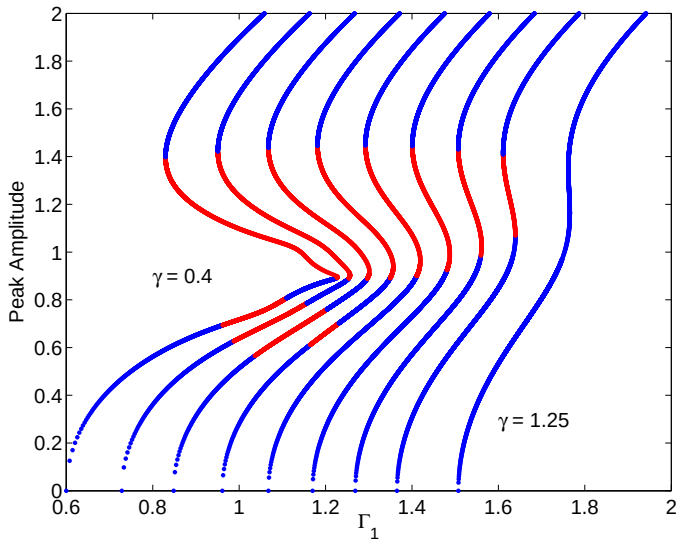

FIG. 5: (Color online) A set of solution branches found in the model with the odd number of intermediate sites, at the following values of the background-loss coefficient (from left to right): $\gamma = 0.4$, 0.5, 0.6, 0.7, 0.8, 0.9, 1, 1.1, 1.25. The parameters are $B = -1$, $E = 0.16$, $\Gamma_2 = 0.8$, and $N_0 = 5$.

Note that the stable mode, into which the unstable one evolves in the middle row of Fig. 8, is qualitatively similar to the one displayed in the upper row of Fig. 4, i.e., it is, most plausibly, an antisymmetric mode corresponding to ansatz (5). Further, the evolution of unstable solutions belonging to the high-amplitude branch leads to the establishment of two fully isolated narrow peaks, see examples in Fig. 9, which is similar to the outcome of the instability development observed in the bottom row of Fig. 4. The instability of these solutions is accounted for by an isolated positive eigenvalues in the linear spectrum, and the emerging stable modes, which feature the isolated peaks, belong to the stable high-amplitude segment, which exists at the same parameter values.

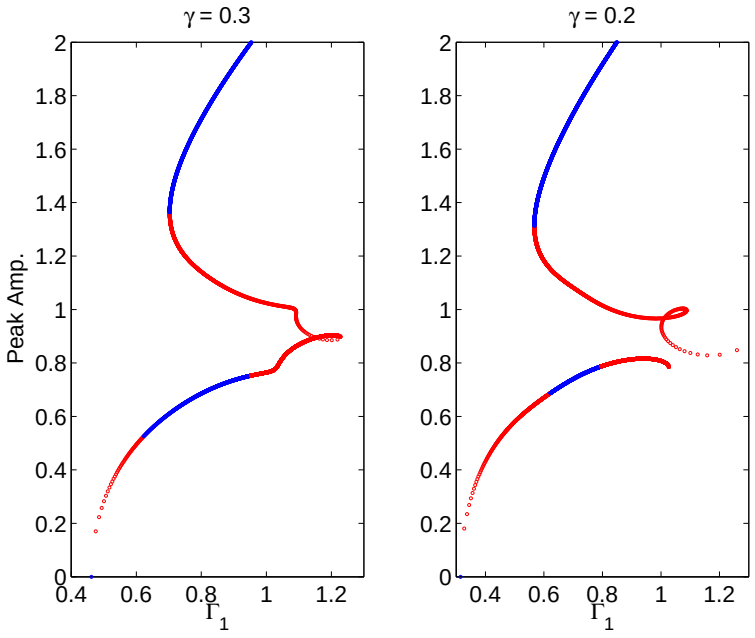

FIG. 6: (Color online) Solution branches at $\gamma = 0.3$ (left) and $\gamma = 0.2$ (right) in the model with the odd number of intermediate sites. Other parameters are as in Fig. 5.

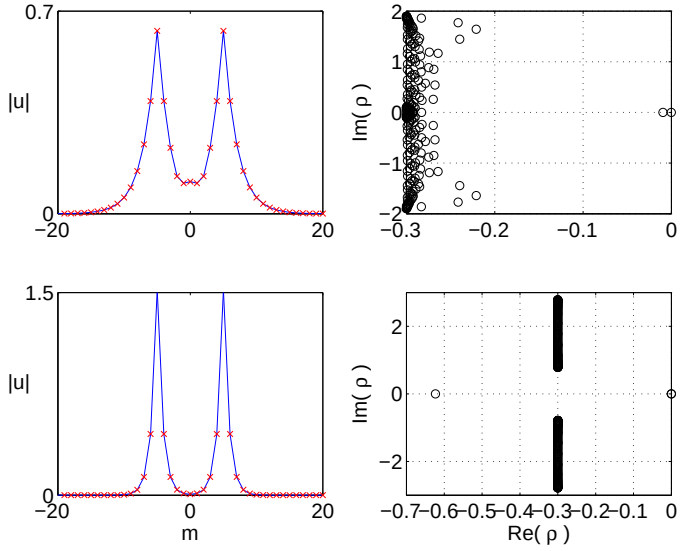

FIG. 7: (Color online) Left: Stable solutions in the model with the odd number of intermediate sites at $\Gamma_1 = 0.7257$ and $\gamma = 0.3$. Right: The corresponding linear-stability spectra.

When the background loss is absent ($\gamma = 0$), solutions in the form of ansatz (3) can only be found in a small region of the parameter space. Figure 10 shows a solution branch in this case. Stable modes exist solely in the region of $0 \leq \Gamma_1 \leq 0.126$. Note that, as it follows from the second equation in system (4), the corresponding wavenumber λ_i in ansatz (3) is zero for stable solutions, and π for unstable ones, i.e., the modes with *staggered* tails, corresponding to $\lambda_i = \pi$, are unstable (in the numerical solution, λ_i can converge to $n\pi$ with other integer values of n, but they all are tantamount to $n = 0$ or 1). The top row of Fig. (11) shows an example of stable solution obtained at $\Gamma_1 = 0.1088$, along with its linear spectrum. On the other hand, the bottom row illustrates what happens in the unstable region. In the absence of the background loss, secondary structures are generated in the course of the evolution as a result of

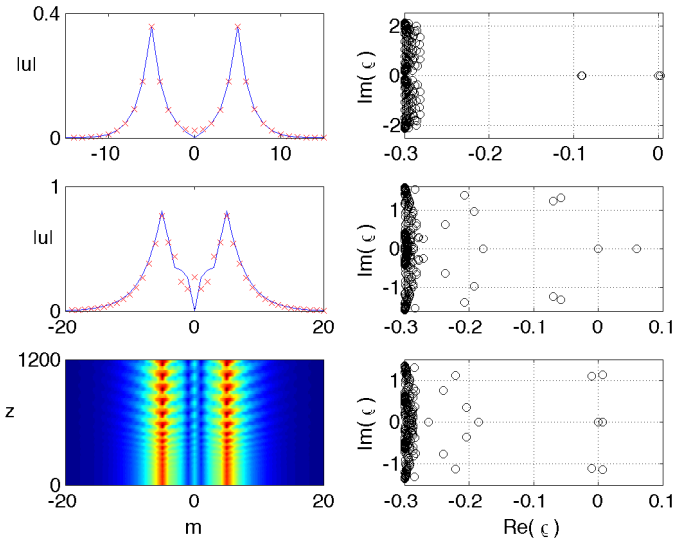

FIG. 8: Left: Unstable solutions produced by the reduced system, and actual stable solutions generated by direct simulations of Eq. (1) at $\gamma = 0.3$ and $\Gamma_1 = 0.5262$ (top), $\Gamma_1 = 1.0053$ (middle), and $\Gamma_1 = 1.0546$ (bottom). In the latter case, the oscillatory instability transforms the stationary pinned mode into a double-peaked breather. Right: The corresponding linear-instability spectra for the solutions produced by the reduced system.

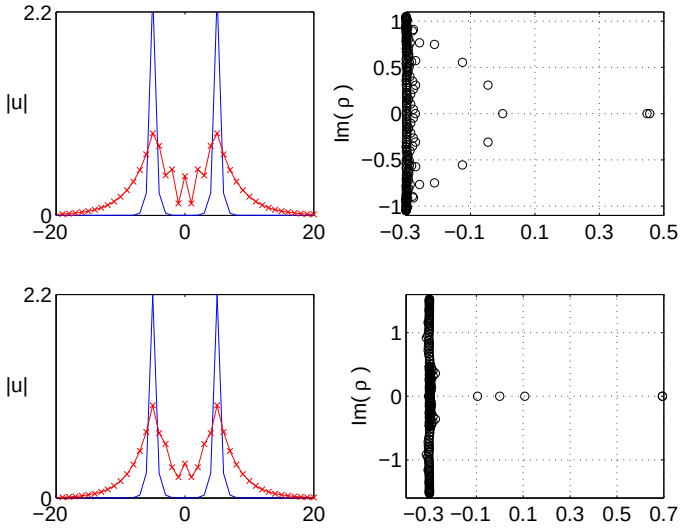

FIG. 9: (Color online) Left: Unstable solutions produced by the reduced system in the model with the odd number of intermediate sites, and the actual stable solutions obtained from direct simulations of Eq. (1) at $\gamma = 0.3$ and $\Gamma_1 = 1.219$ (top), and $\Gamma_1 = 1.087$ (bottom). Right: The corresponding linear-instability spectra.

the emission of lattice waves ("phonons"). The positive eigenvalue in the spectrum is a signature of the instability.

It is worth mentioning that, since $\lambda_i = 0$ or $\lambda_i = \pi$ when $\gamma = 0$, the real and imaginary parts of the last equation in system (4) give

$$\Gamma_1/E = |A|^2 e^{-2\lambda_r N_0} , \tag{11}$$

$$\Gamma_2 + B|A|^2 e^{-2\lambda_r N_0} = \pm \frac{\sinh(\lambda_r)}{1 + e^{-2\lambda_r N_0}} , \tag{12}$$

where the plus and minus signs correspond to $\lambda_i = 0$ and $\lambda_i = \pi$, respectively. These equations can be combined to

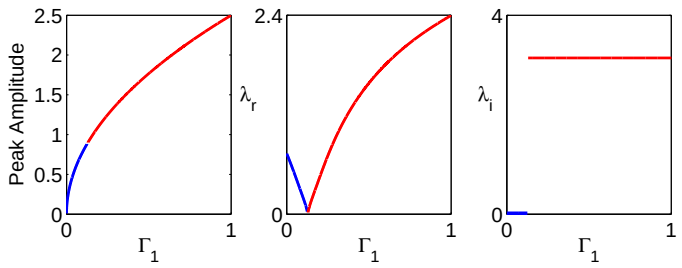

FIG. 10: (Color online) Characteristics of the solution branch in the model with an odd number of intermediate sites and $\gamma = 0$ (no background loss).

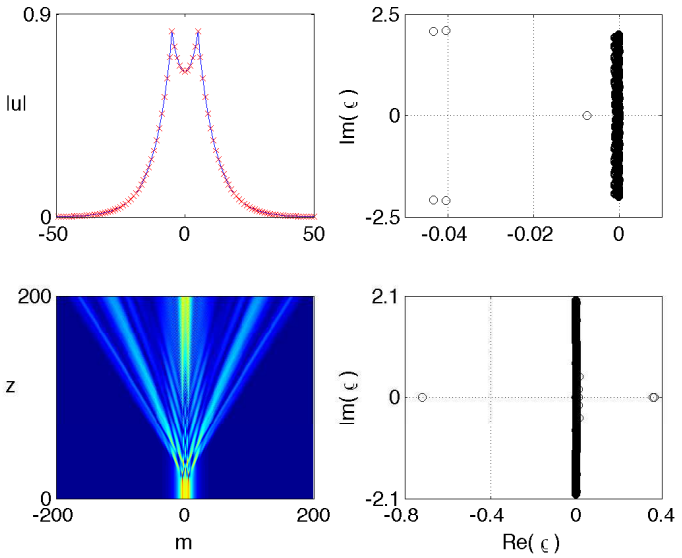

FIG. 11: (Color online) Left: Stable (top) and unstable (bottom) solutions obtained from the full equation (1) and reduced model (4) in the system with the odd number of intermediate sites and $\gamma = 0$, for $\Gamma_1 = 0.1088$ and $\Gamma_1 = 0.1434$, respectively. Right: The corresponding linear-stability spectra.

yield

$$\Gamma_2 + \frac{B\Gamma_1}{E} = \frac{\pm \sinh \lambda_r}{1 + e^{-2\lambda_r N_0}} \, . \tag{13}$$

One can solve Eq. (13) for linear gain Γ_1 in terms of λ_r, and, subsequently, the remaining solution parameters. A and C, can be easily found from the other equations of system (4).

B. An even number of intermediate sites between the hot spots

We have also studied the linear stability of solutions obtained in the form of ansatz (7), whose parameters were found from a numerical solution of reduced system (8). For the same parameters as adopted above (i.e., $N_0 = 5$, $B = -1$, $E = 0.16$, $\Gamma_2 = 0.8$) and in the presence of the background loss ($\gamma > 0$), it has been found that the solution branches and their stability resemble those reported in the previous section (which is quite natural, as the two-peak modes of the two types should be close for the numbers of the intermediate sites $N_{\rm odd} \equiv 2N_0 - 1 = 9$ and $N_{\rm even} \equiv 2\,(N_0 - 1) = 8$), therefore we do not discuss the results for $N_{\rm even}$ in detail here. It is relevant to point out that, in the case of $\gamma = 0$ (no background loss), one can again obtain an explicit relation between the linear gain Γ_1

and the inverse width λ_r, which is similar to Eq. (13):

$$\Gamma_2 + \frac{B\Gamma_1}{E} = \frac{\pm \sinh \lambda_r}{1 \pm e^{-2\lambda_r(N_0-1/2)}}. \tag{14}$$

Here, as before, the plus and minus signs correspond to $\lambda_i = 0$ and $\lambda_i = \pi$, respectively.

A specific particular case is the one when the two HSs are set at adjacent sites of the lattice, without intermediate sites between them ($N_{\rm even} = 0$), which corresponds to $N_0 = 1$ in Eqs. (6) and (7). Figure 12 shows examples of stationary solutions for this case. Obviously, their shape does not feature distinct peaks, in contrast with the profile depicted in Fig. 3. However, the stability is similar to that for $N_0 > 1$, stable solutions being found for small and large values of Γ_1, while breathers are observed at intermediate values of Γ_1, as a result of the Hopf bifurcation, see Fig. 12.

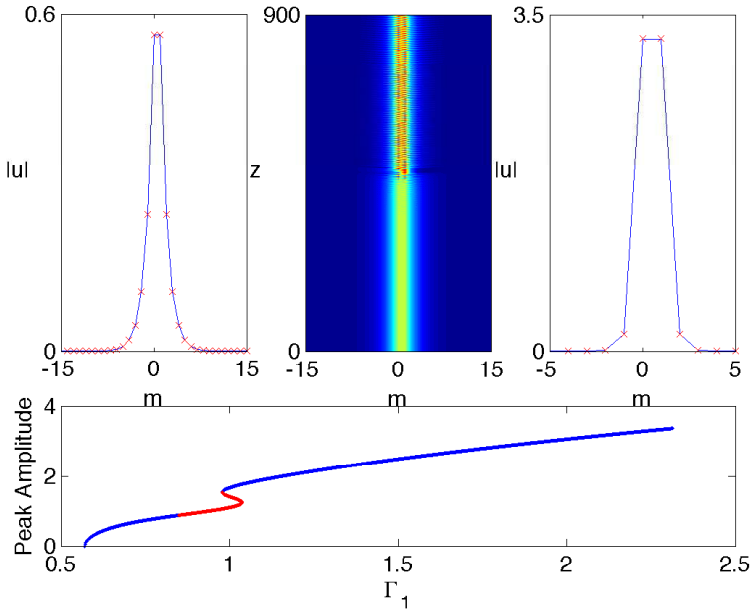

FIG. 12: (Color online) The top left and right panels: examples of stable stationary modes supported by two adjacent hot spots (as obtained from both direct simulations and solution of the reduced system (8)), at $\Gamma_1 = 0.6656$ and $\Gamma_1 = 2.186$, respectively. The top middle panel: a breather revealed by the direct simulations at $\Gamma_1 = 0.9099$. Other parameters are $N_0 = 1$, $B = -1$, $E = 0.16$, $\Gamma_2 = 0.8$, and $\gamma = 0.5$. The bottom panel displays the corresponding solution branch, with an unstable (red) segment in the middle.

V. CONCLUSION

We have introduced an analytically tractable discrete dissipative model, in which stationary modes are supported by a symmetric pair of embedded HSs (hot spots), represented by two sites carrying the linear gain, self-defocusing nonlinearity, and cubic loss. The system can be readily implemented in photonics and plasmonics, using waveguiding arrays, with the gain and nonlinearity applied to two cores, which are chosen as HSs. Symmetric solutions were obtained in an implicit analytical form, separately for odd and even numbers of intermediate sites between the two HSs, $N_{\rm odd}$ and $N_{\rm even}$. The latter case includes the configuration with adjacent HSs ($N_{\rm even} = 0$). The modes with $N_{\rm odd}$ feature both the simple shape, with a minimum at the center, and the w-shaped one, with an additional lower peak at the central point. The linear stability of the stationary solutions was investigated in the numerical form, which has revealed both stable and unstable portions of the solution families. In most cases when the instability is accounted for by isolated real positive eigenvalues, direct simulations demonstrate that the unstable mode spontaneously evolves into a stable one, which can be found at the same parameter values. However, in some cases the evolution transforms unstable symmetric modes into apparently antisymmetric stable solutions. The instability represented by a pair of complex conjugate eigenvalues gives rise to persistent breathers.

The same model may give rise to antisymmetric solutions, which will be reported elsewhere (it appears that, in some cases, unstable symmetric modes may evolve into stable antisymmetric ones). A challenging issue, which will be studied separately, is to search for asymmetric modes, with unequal amplitudes at the positions of the two symmetric HSs.

Acknowledgment

A partial financial support for this project has been provided by the University of Hong Kong Incentive Award Scheme.

[1] N. N. Rosanov, *Spatial Hysteresis and Optical Patterns* (Springer: Berlin, 2002).
[2] N. Lazarides and G. P. Tsironis, Phys. Rev. E **71**, 036614 (2005); Y. M. Liu, G. Bartal, D. A. Genov, and X. Zhang, Phys. Rev. Lett. **99**, 153901 (2007); E. Feigenbaum and M. Orenstein, Opt. Lett. **32**, 674 (2007); I. R. Gabitov, A. O. Korotkevich, A. I. Maimistov, and J. B. Mcmahon, Appl. Phys. A **89**, 277 (2007); A. R. Davoyan, I. V. Shadrivov, and Y. S. Kivshar, Opt. Exp. **17**, 21732 (2009); K. Y. Bliokh, Y. P. Bliokh, and A. Ferrando, Phys. Rev. A **79**, 041803 (2009); E. V. Kazantseva and A. I. Maimistov, *ibid.* **79**, 033812 (2009); Y.-Y. Lin, R.-K. Lee, and Y. S. Kivshar, Opt. Lett. **34**, 2982 (2009); A. Marini and D. V. Skryabin, *ibid.* **81**, 033850 (2010).
[3] A. Marini, D. V. Skryabin, and B. A. Malomed, Opt. Exp. **19**, 6616 (2011).
[4] J. N. Kutz and B. Sanstede, Opt. Exp. **16**, 636 (2008); M. O. Williams and J. N. Kutz, *ibid.* **17**, 18320 (2009).
[5] B. A. Malomed and H. G. Winful, Phys. Rev. E **53**, 5365 (1996); J. Atai and B. A. Malomed, Phys. Rev. E **54**, 4371 (1996); H. Sakaguchi and B. A. Malomed, Physica D **147**, 273 (2000).
[6] P. V. Paulau D. Gomila, P. Colet, N. A. Loiko, N. N. Rosanov, T. Ackemann, and W. J. Firth, Opt. Exp. **18**, 8859 (2010).
[7] B. A. Malomed, Chaos **17**, 037117 (2007).
[8] B. A. Malomed, Physica D **29**, 155 (1987); O. Thual and S. Fauve, J. Phys. (France) **49**, 1829 (1988); W. van Saarloos and P. Hohenberg, Phys. Rev. Lett. **64**, 749 (1990); V. Hakim, P. Jakobsen and Y. Pomeau, Europhys. Lett. **11**, 19 (1990); B. A. Malomed and A. A. Nepomnyashchy, Phys. Rev. A **42**, 6009 (1990); P. Marcq, H. Chaté, and R. Conte, Physica D **73**, 305 (1994); T. Kapitula and B. Sandstede, J. Opt. Soc. Am. B **15**, 2757 (1998).
[9] N. N. Akhmediev, V. V. Afanasjev, J. M. Soto-Crespo, and S. Wabnitz, Phys. Rev. Lett. **79**, 4047 (1997); A. Komarov, H. Leblond, and F. Sanchez, Phys. Rev. E **72**, 025604 (2005); J. N. Kutz, SIAM Rev. **48**, 629 (2006); W. Renninger, A. Chong, and F. Wise, Phys. Rev. A **77**, 023814 (2008); E. Ding and J. N. Kutz, J. Opt. Soc. Am. B **26**, 2290 (2009).
[10] W. C. K. Mak, B. A. Malomed, and P. L. Chu, Phys. Rev. E **67**, 026608 (2003).
[11] C.-K. Lam, B. A. Malomed, K. W. Chow, and P. K. A. Wai, Eur. Phys. J. Special Topics **173**, 233 (2009).
[12] Y. V. Kartashov, V. V. Konotop, and V. A. Vysloukh, EPL **91**, 34003 (2010).
[13] O. V. Borovkova, V. E. Lobanov, and B. A. Malomed, EPL **97**, 44003 (2012).
[14] C. H. Tsang, B. A. Malomed, C.-K. Lam, and K. W. Chow, Eur. Phys. J. D **59**, 81 (2010)
[15] D. A. Zezyulin, Y. V. Kartashov, and V. V. Konotop, Opt. Lett. **36**, 1200 (2011); Y. V. Kartashov, V. V. Konotop, and V. A. Vysloukh, Phys. Rev. A **83**, 041806(R) (2011); D. A. Zezyulin, V. V. Konotop, and G. L. Alfimov, Phys. Rev. E **82**, 056213 (2010).
[16] C. H. Tsang, B. A. Malomed, and K. W. Chow, Phys. Rev. E **84**, 066609 (2011).
[17] D. A. Zezyulin, G. L. Alfimov, and V. V. Konotop, Phys. Rev. A **81**, 013606 (2010); F. K. Abdullaev, V. V. Konotop, M. Salerno, and A. V. Yulin, Phys. Rev. E **82**, 056606 (2010).
[18] J. Hukriede, D. Runde, and D. Kip, J. Phys. D: Appl. Phys. **36**, R1 (2003).
[19] V. Skarka, N. B. Aleksić, H. Leblond, B. A. Malomed, and D. Mihalache, Phys. Rev. Lett. **105**, 213901 (2010); V. E. Lobanov, Y. V. Kartashov, V. A. Vysloukh, and L. Torner, Opt. Lett. **36**, 85 (2011); O. V. Borovkova, V. E. Lobanov, Y. V. Kartashov, and L. Torner, *ibid.* **36**, 1936 (2011); O. V. Borovkova, Y. V. Kartashov, V. E. Lobanov, V. A. Vysloukh, and L. Torner, *ibid.* **36**, 3783 (2011); O. V. Borovkova, V. E. Lobanov, Y. V. Kartashov, and L. Torner, *ibid.* **36**, 1936 (2011).
[20] B. A. Malomed, E. Ding, K. W. Chow and S. K. Lai, Phys. Rev. E **86**, 036608 (2012).
[21] M. I. Molina and G. Tsironis, Phys. Rev. B **47**, 15330 (1993); B. C. Gupta and K. Kundu, *ibid.* **55**, 894 (1997).
[22] V. A. Brazhnyi and B. A. Malomed, Phys. Rev. A **83**, 053844 (2011).